

Traffic Signal Optimization on a Square Lattice using the D-Wave Quantum Annealer

Daisuke Inoue,* Akihisa Okada, Tadayoshi Matsumori, and Hiroaki Yoshida
Toyota Central R&D Labs., Inc.
Bunkyo-ku, Tokyo 112-0004, Japan

Kazuyuki Aihara
The University of Tokyo
Bunkyo-ku, Tokyo 113-0033, Japan

The spread of intelligent transportation systems in urban cities has caused heavy computational loads, requiring a novel architecture for managing large-scale traffic. In this study, we develop a method for globally controlling traffic signals arranged on a square lattice by means of a quantum annealing machine, namely the D-Wave quantum annealer. We first formulate a signal optimization problem that minimizes the imbalance of traffic flows in two orthogonal directions. Then we reformulate this problem as an Ising Hamiltonian, which is fully compatible with quantum annealers. The new control method is compared with a conventional local control method for a large 50-by-50 city, and the results exhibit the superiority of our global control method in suppressing traffic imbalance over wide parameter ranges. Furthermore, the solutions to the global control method obtained with the quantum annealing machine are better than those obtained with conventional simulated annealing. In addition, we prove analytically that the local and the global control methods converge at the limit where cars have equal probabilities for turning and going straight. These results are verified with numerical experiments.

INTRODUCTION

For the last two decades, intelligent and efficient transportation systems have been developing, and therefore, control methods for cooperative management of such systems have become increasingly important [1–3]. In particular, optimal operation of traffic lights is crucial for avoiding stagnation of traffic flows [4, 5]. In a large city, however, simultaneously controlling a huge number of traffic lights requires significant computational costs. Various methods to circumvent this difficulty have been proposed, and they mainly focus on distributed optimization with divisions of the system or by regarding signals as multi-agents [6–13]. In these methods, global optimization is sacrificed to divide the problem, and therefore, an alternative computational technique is necessary to guarantee global optimality. As a novel computational method specifically designed to solve an optimization problem, *quantum annealing* has rapidly attracted much attention [14–16], particularly after D-Wave Systems Inc. released a relatively large-scale commercial machine, quantum annealer 2000Q. The quantum annealing machine uses a natural phenomenon called quantum fluctuation to solve optimization problems, and it is expected to provide accurate solutions with short computational times, compared with conventional Neumann-type machines. However, restrictions on the number of available variables and the class of solvable problems still hinder the expansion of practical applications, and the search for applications exploiting the power of this computer is becoming an active research area [17–21].

In this paper, we propose a method for globally controlling traffic signals in an urban city using the quantum annealer 2000Q. We consider a situation in which many cars moving on a lattice network are controlled via traffic signals installed at each intersection. To analytically handle this network, we consider a simplified situation in which two states are assumed for each signal: traffic is allowed in either the north-south direction or the east-west direction. The cars moving on the lattice are assumed to choose whether to make a turn or to go straight at an intersection with a given probability. We then formulate the signal operation problem as a combinatorial optimization problem. The objective function of the formulated problem is shown to be formally consistent with the Hamiltonian of the *Ising model*. The Ising model is a statistical ferromagnetism physics model that represents the behavior of a spin system, and it captures the relation between the microscopic state of spins and the macroscopic phenomena of magnetic phase transitions [22–25]. Importantly, reformulation of the problem with the Ising model is fully compatible with the class of problems that the 2000Q accepts; hence, one can apply quantum annealing to solve the signal optimization problem.

By reformulating the problem using Ising minimization, this study makes three contributions to signal optimization. First, by performing numerical experiments, we confirm the engineering effectiveness of the proposed method using quantum annealing. Results of experiments using a large city consisting of 50×50 intersections show that the proposed

* daisuke-inoue@mosk.tytlabs.co.jp

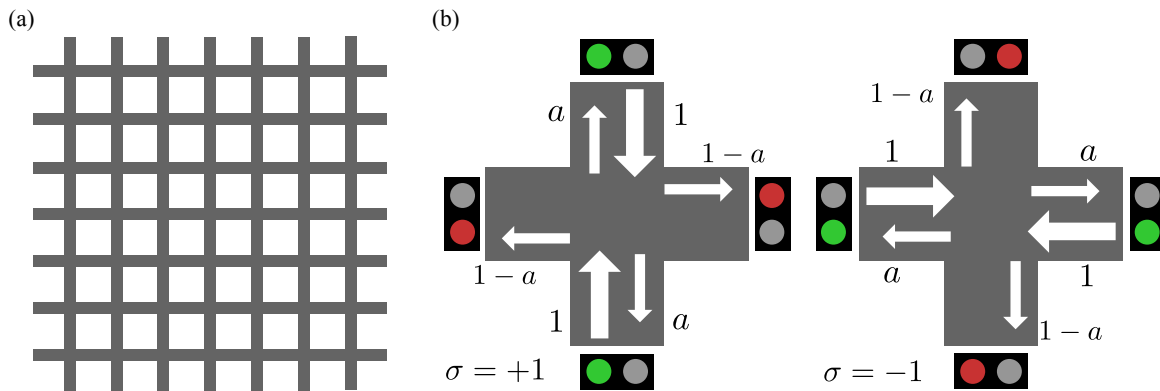


FIG. 1. Traffic signal model. (a) Grid pattern of roads. (b) The two states of traffic signals at each intersection. In the case of $\sigma = +1$, the vehicles coming from the horizontal direction stop, and the vehicles coming from the vertical direction go straight at the rate of a , turn right at the rate of $(1-a)/2$, and turn left at the rate of $(1-a)/2$. The rate $1-a$ shown for the horizontal direction is the sum of the vehicles from the two vertical directions. In the case of $\sigma = -1$, the roles of the vertical and horizontal directions are reversed.

method achieves signal operation close to the global optimal solution, compared with the results of a conventional local control method [26]. The reformulated optimization problem is also solved using a classical simulated annealing method, but the quantum annealing machine is found to give a better solution in a specific parameter domain. Second, a theoretical correspondence between local and global control methods is found. Specifically, we analytically show that the conventional local control is consistent with the solution of the global signal optimization problem at the limit where the probability of cars going straight is equal to the probability of them turning. This result provides a theoretical basis for the numerical prediction of a previous study [26], where the local control is found to cause phase transitions similar to those of the Ising model. The last contribution is the knowledge gained for the cooperative operation of traffic signals. Our numerical experiments show a strong correlation between a signal and its neighboring signals. In addition, a strong temporal correlation of signals emerges, that is, the signal display at a certain time is correlated with the displays in the previous several steps. This spatio-temporal correlation becomes stronger as the straight driving probability of the cars increases. Our results suggest the necessity of signal cooperation for smooth traffic flow, with variation of cooperation strength depending on the rate at which vehicles drive straight.

RESULTS

Traffic Signal Optimization Problem

Consider $L \times L$ ($L \in \mathbb{N}$) roads arranged in east-west and north-south directions with a periodic boundary condition. Each road consists of two lanes, one in each direction. Traffic signals are located at each intersection to control the flow of vehicles traveling on the roads. The signal at each node i has one of two states: $\sigma_i = +1$, which allows vehicle flow only in the north-south direction, and $\sigma_i = -1$, which allows vehicle flow only in the east-west direction. Each car goes straight through each intersection at fixed probability $a \in [0, 1]$ and otherwise turns to the left or right with equal probabilities, that is, $(1-a)/2$ for each direction. Figure 1 illustrates this situation.

Reference [26] shows that the number of vehicles $q_{ij} \in \mathbb{R}_+$ in the traffic lane from intersection j to i evolves according to the following difference equation:

$$q_{ij}(t+1) = q_{ij}(t) + \frac{s_{ij}}{2}(-\sigma_i + \alpha\sigma_j), \quad (1)$$

where $\alpha := 2a - 1$, and $s_{ij} \in \{\pm 1\}$ is the direction of the lane from node j to i ; here, $s_{ij} = +1$ denotes north-south and $s_{ij} = -1$ denotes east-west. We note here that q_{ij} is normalized by the number of cars passing per unit of time. Precisely, in terms of the mean flux of moving cars Q_{av} and the dimensional time unit Δt , $t = t^*/\Delta t$ and $q_{ij} = q_{ij}^*/(Q_{av}\Delta t)$, where t^* is the dimensional time and q_{ij}^* is the number of vehicles in a lane. We define a quantity

that represents the deviation of the north-south flow and the east-west flow at each intersection i as

$$x_i(t) := \sum_{j \in \mathcal{N}(i)} \frac{s_{ij} q_{ij}(t)}{2}, \quad (2)$$

where $\mathcal{N}(i)$ represents the index of the four intersections adjacent to intersection i . Equation (2) transforms Eq. (1) into a time evolution equation for the flow bias $x(t)$ as follows:

$$\mathbf{x}(t+1) = \mathbf{x}(t) + \left(-I + \frac{\alpha}{4}A\right) \boldsymbol{\sigma}(t), \quad (3)$$

where the flow bias vector is defined as $\mathbf{x} := [x_1, \dots, x_{L \times L}]^\top$ and the signal state vector is defined as $\boldsymbol{\sigma} := [\sigma_1, \dots, \sigma_{L \times L}]^\top$. The matrix $A \in \mathbb{R}^{L^2 \times L^2}$ is the adjacent matrix of the periodic lattice graph.

Next, we define the following objective function to evaluate traffic conditions at each time step:

$$H(\boldsymbol{\sigma}(t)) := \mathbf{x}(t+1)^\top \mathbf{x}(t+1) + \eta(\boldsymbol{\sigma}(t) - \boldsymbol{\sigma}(t-1))^\top (\boldsymbol{\sigma}(t) - \boldsymbol{\sigma}(t-1)), \quad (4)$$

where the first term on the right-hand side suppresses the flow bias during the next time step at each intersection, the second term prevents the traffic signal state at each intersection from switching too frequently, and $\eta \in \mathbb{R}_+$ is a weight parameter for determining the ratio of the two terms. The traffic signal state $\sigma_i(t)$ at each time step is determined so that the objective function (4) is minimized; that is, we want to find the value of $\bar{\boldsymbol{\sigma}}(t)$ that satisfies

$$\bar{\boldsymbol{\sigma}}(t) = \arg \min_{\boldsymbol{\sigma} \in \{\pm 1\}^{L \times L}} H(\boldsymbol{\sigma}(t)). \quad (5)$$

Ising Formulation and Optimization

Substituting Eq. (3) into Eq. (4) gives the following representation:

$$H(\boldsymbol{\sigma}(t)) = \left(\mathbf{x}(t) + \left(-I + \frac{\alpha}{4}A\right) \boldsymbol{\sigma}(t)\right)^\top \left(\mathbf{x}(t) + \left(-I + \frac{\alpha}{4}A\right) \boldsymbol{\sigma}(t)\right) + \eta(\boldsymbol{\sigma}(t) - \boldsymbol{\sigma}(t-1))^\top (\boldsymbol{\sigma}(t) - \boldsymbol{\sigma}(t-1)) \quad (6)$$

$$= \boldsymbol{\sigma}(t)^\top \left(\left(-I + \frac{\alpha}{4}A\right)^\top \left(-I + \frac{\alpha}{4}A\right) + \eta I \right) \boldsymbol{\sigma}(t) + \left(2\mathbf{x}(t)^\top \left(-I + \frac{\alpha}{4}A\right) - 2\eta\boldsymbol{\sigma}(t-1)^\top\right) \boldsymbol{\sigma}(t) + c(t), \quad (7)$$

where $c(t)$ is a constant term that does *not* include $\boldsymbol{\sigma}(t)$. By defining the variables

$$J := \left(-I + \frac{\alpha}{4}A\right)^\top \left(-I + \frac{\alpha}{4}A\right) + \eta I, \quad (8)$$

$$h := 2\mathbf{x}(t)^\top \left(-I + \frac{\alpha}{4}A\right) - 2\eta\boldsymbol{\sigma}(t-1)^\top, \quad (9)$$

we can represent the objective function (6) as follows:

$$H(\boldsymbol{\sigma}(t)) = \boldsymbol{\sigma}(t)^\top J \boldsymbol{\sigma}(t) + h \boldsymbol{\sigma}(t) + c(t). \quad (10)$$

Equation (10) is a quadratic form with variables $\{\pm 1\}$, which matches the Hamiltonian form of the Ising model [22]. Hence, solving the signal optimization problem of the objective function (4) is regarded as equivalent to the problem of finding the spin direction $\sigma_i \in \{\pm 1\}$ that minimizes the Ising Hamiltonian of Eq. (10). Because the Ising Hamiltonian is fully compatible with the class of problems that the 2000Q accepts, quantum annealing can be applied to solve the signal optimization problem.

We use a city consisting of 50×50 intersections to consider the signal operation problem, and we compare the results of numerical experiments on the following three methods for traffic control:

- Local control, which determines the signal display at each time step with the following local rules:

$$\begin{cases} \sigma_i(t) \leftarrow +1 & \text{if } x_i(t) \geq +\theta, \\ \sigma_i(t) \leftarrow -1 & \text{if } x_i(t) \leq -\theta. \end{cases} \quad (11)$$

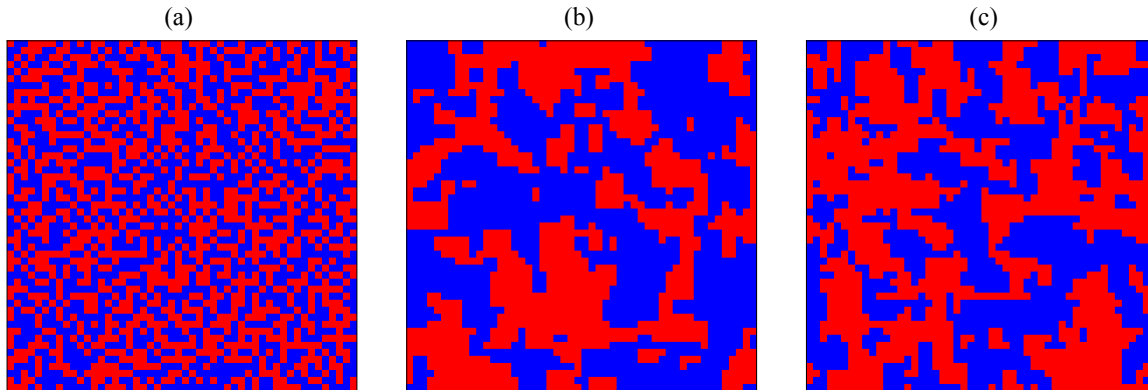


FIG. 2. Snapshots of traffic signals under different control methods. (a) Local controller using Eq. (11), (b) Global controller optimizing Eq. (10) with simulated annealing, and (c) Global controller optimizing Eq. (10) with the D-Wave 2000Q. Red and blue dots represent vertical and horizontal directions allowed at each crossing, respectively. Parameters α , η , and L are fixed as $\alpha = 0.8$, $\eta = 1.0$, and $L = 50$, respectively. For the D-Wave method, the Hamiltonian is divided into 42 groups and the optimization problem is solved in parallel. See *Methods* for details.

Equation (11) switches the display of the traffic signals to reduce the flow bias when the magnitude of the bias becomes larger than the threshold value $\theta \in \mathbb{R}_+$ at each intersection. To compare the local control with the optimal control, the value of the switching parameter θ is determined such that the common objective function (4) is minimized. For details, refer to *Methods*.

- Optimal control with simulated annealing, which reduces Eq. (10) at each time step using *simulated annealing*. Simulated annealing is an algorithm for finding a solution by examining the vicinity of the current solution at each step and probabilistically determining whether it should stay in the current state or switch to a vicinity state. See Ref. [27] for details of simulated annealing. We used the *anneal* library provided by D-Wave for executing this algorithm.
- Optimal control with quantum annealing, which reduces Eq. (10) by using quantum annealing with the D-Wave 2000Q. Because the problem size exceeds the size of problems that 2000Q can solve, it is subdivided by the *graph partitioning* technique. We used the *ocean* library provided by D-Wave for executing this algorithm. See *Methods* for the detailed procedure.

Figure 2 shows snapshots of the signal display at time $t = 100$ for $\alpha = 0.8$ and $\eta = 1.0$, where α is the parameter related to vehicle's straight driving probability and η is the weight parameter in the objective function (4). The flow bias distribution at the initial time $\mathbf{x}(0)$ are generated as random numbers following a uniform distribution of $[-5.0, 5.0]$, and the signal states at the initial time $\boldsymbol{\sigma}(0)$ are generated as random numbers following a binomial distribution of $\{\pm 1\}$. In Fig. 2, blue dots mean that the cars are allowed to pass in the east-west direction, and red dots mean that the cars are allowed to pass in the north-south direction. We observe the synchronization of proximity signals under optimal control [see Figs. 2(b, c)], while the two direction states are distributed rather uniformly under local control [see Fig. 2(a)].

Figure 3(a) plots the time evolution of the Hamiltonian of Eq. (10) for each method when $\alpha = 0.8$ and $\eta = 1.0$. In all three methods, the signals change rapidly over time to reduce the Hamiltonian. The value of the Hamiltonian in the steady state is the smallest in the quantum annealing method, followed by the simulated annealing method, and it is the largest under local control. That is, optimal control using quantum annealing exhibits the best performance among the three methods.

We examine the effect of changing the parameter α , the vehicle's straight driving probability, on the Hamiltonian of Eq. (10). The time average of the Hamiltonian of Eq. (10), denoted as \bar{H} , is plotted in Fig. 3(b). As α approaches zero, the values of the Hamiltonian for the local and optimal control methods converge to a common value. This suggests that local control gives the solution to the signal optimization problem at the limit of $\alpha \rightarrow 0$. The validity of this conjecture is explored in *Discussion*. In the interval of $\alpha \in [0.2, 0.8]$, the Hamiltonian under optimal control is smaller than that under local control, showing that the optimum control method exhibits performance better than that of local control in this range. However, in the simulated annealing method at $\alpha > 0.8$, the value of the Hamiltonian is larger than that under the local control method, suggesting that simulated annealing does *not* reach the global

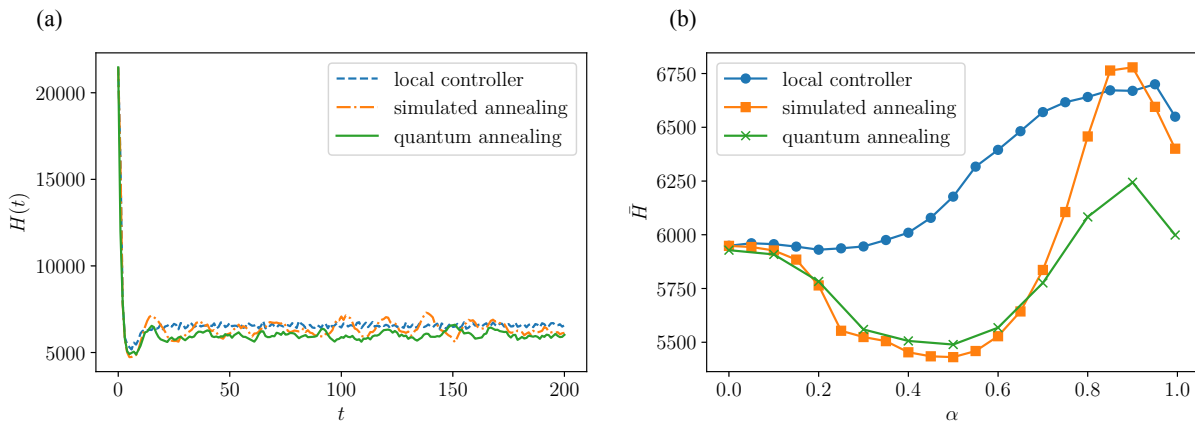


FIG. 3. Hamiltonian of Eq. (10) under different control methods. (a) Time evolution of the Hamiltonian, where the parameters α, η , and L are fixed as $\alpha = 0.8, \eta = 1.0$, and $L = 50$, respectively. (b) Time average of Hamiltonian as functions of α , where the parameters η and L are the same as those in (a).

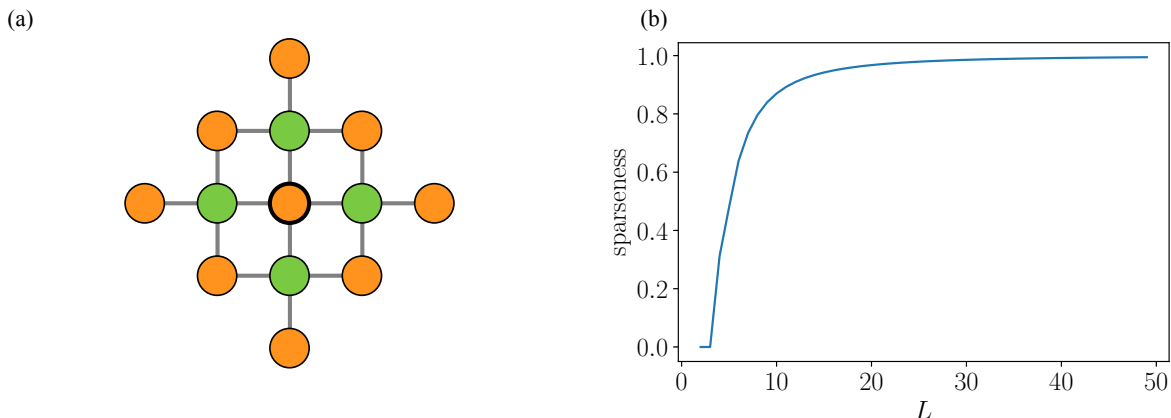


FIG. 4. Sparseness of the matrix J in Eq. (8). (a) Nodes neighboring the reference node (green) and two nodes away from the reference node (orange) in a lattice graph. (b) Sparseness $S_J(L)$ of Eq. (13) for different numbers of intersections L .

optimal solution. Conversely, under the quantum annealing method, the value of the Hamiltonian is smaller than that under the other two methods, which means that the solution is closer to the global optimum.

DISCUSSION

Performance Analysis of Quantum Annealing. The performance of the D-Wave 2000Q is known to vary depending on the structure of the problem. In particular, when the matrix J in Eq. (8) has a sparse structure, the accuracy of the solution is improved [28]. To check the sparseness of our formulated problem, we examine the value of all components of J in Eq. (8). First, expanding J yields the following expression:

$$J = (1 + \eta)I - \frac{\alpha}{2}A + \frac{\alpha^2}{16}A^\top A, \quad (12)$$

where the number of non-zero elements in each column of A is 4, because it is equal to the number of degrees of each node in the lattice graph [see the green nodes in Fig. 4(a)]. Also, the number of non-zero elements in each column of $A^\top A$ is 9 because it coincides with the number of nodes two nodes away from the reference node in the lattice graph [see the orange nodes in Fig. 4(a)]. Thus, the number of all non-zero elements in J is expressed as $13L^2$. From this, we calculate $S_J(L)$, the sparseness of matrix J , defined as the ratio of the number of 0-valued elements and the number of

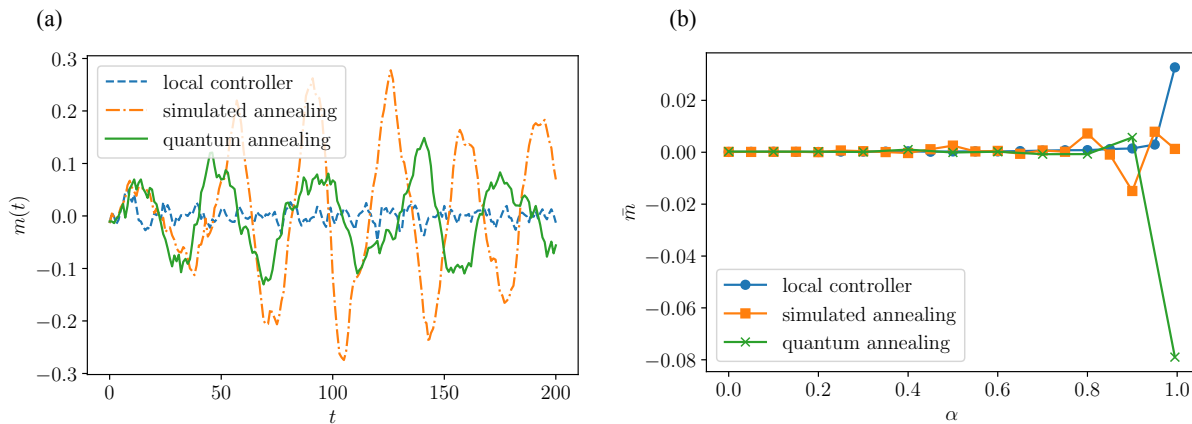


FIG. 5. Magnetization of Eq. (18) under different control methods. (a) Time evolution of magnetization. Parameters α , η , and L are fixed as $\alpha = 0.8$, $\eta = 1.0$, and $L = 50$, respectively. (b) Time average of magnetization as a function of α . Parameters η and L are the same as those in (a).

all elements in the matrix:

$$S_J(L) = \frac{L^4 - 13L^2}{L^4}, \quad (13)$$

where we confirm that $S_J(L) \rightarrow 1$ as $L \rightarrow \infty$. In Fig. 4(b), we plot $S_J(L)$ given in Eq. (13), to show that the sparseness of matrix J increases as increasing city size. This allows us to expect that the performance of the D-Wave 2000Q is enhanced in the case of the signal optimization problem for a rather large cities, such as $L = 50$, the one considered in the present paper.

Local and Optimal Control Correspondence. As shown in Fig. 5, when the parameter α of Eq. (1) is sufficiently small, the local control of Eq. (11) approaches the optimal control that is the solution of Eq. (5). When $\alpha \approx 0$ is valid, the term associated with α in Eq. (10) can be ignored, yielding

$$J \approx (1 + \eta)I, \quad (14)$$

$$h \approx -2\mathbf{x}(t)^\top - 2\eta\boldsymbol{\sigma}(t-1)^\top. \quad (15)$$

Because J in Eq. (14) is a diagonal matrix, the first term $\boldsymbol{\sigma}(t)^\top J \boldsymbol{\sigma}(t)$ on the right-hand side of Eq. (10) is a constant that does *not* depend on $\boldsymbol{\sigma}$. Therefore, the minimizer of $H(\boldsymbol{\sigma}(t))$ is determined depending only on the sign of h in Eq. (15), that is,

$$\bar{\sigma}_i(t) = \begin{cases} 1 & \text{if } x_i(t) + \eta\sigma_i(t-1) \geq 0, \\ -1 & \text{if } x_i(t) + \eta\sigma_i(t-1) < 0, \end{cases} \quad (16)$$

for all $i = 1, \dots, L \times L$. By transforming Eq. (16), we obtain

$$\bar{\sigma}_i(t) = \begin{cases} 1 & \text{if } x_i(t) \geq \eta, \\ -1 & \text{if } x_i(t) \leq -\eta, \\ \sigma(t-1) & \text{otherwise,} \end{cases} \quad (17)$$

for all $i = 1, \dots, L \times L$. The control method of Eq. (17) is equivalent to the local control (11) in Ref. [26].

Because $\alpha = 0 \Leftrightarrow a = 0.5$ holds, this optimality means that an appropriate vehicle turning rate autonomously eases the flow bias in the local control laws. In addition, the occurrence of this magnetic transition for the signal display, stated in Ref. [26], is consistent with the fact that local control in Eq. (11) actually minimizes the Ising Hamiltonian in Eq. (10). However, note that the optimality of local control is valid only when $\alpha \approx 0$, but *not* when $\alpha \rightarrow 1$, where the phase transition occurs.

Signal Synchronization Analysis. To analyze the signal correlation observed in Fig. 2, we calculate the magnetization,

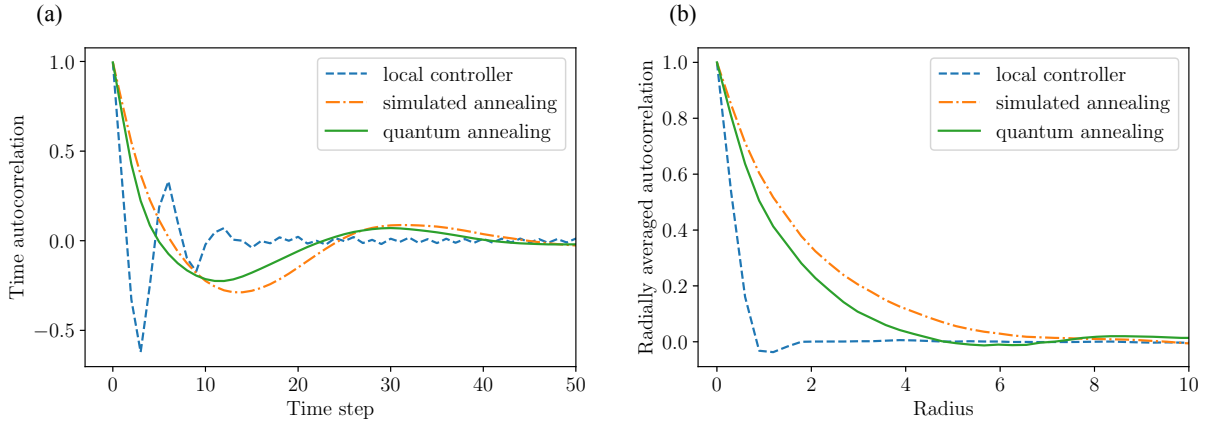


FIG. 6. Time and spatial autocorrelation functions for different control methods. (a) Time autocorrelation function and (b) Radially averaged spatial autocorrelation function. Parameters α , η , and L are fixed as $\alpha = 0.8$, $\eta = 1.0$, and $L = 50$, respectively.

which is regarded as an important quantity in the Ising model:

$$m(t) := \frac{1}{L^2} \sum_{i=1}^{L^2} \sigma_i(t). \quad (18)$$

In the Ising model, this value represents the spin bias of the entire system, and it is an indicator of ferromagnetic transitions in the system. Figure 5(a) shows the time variation of magnetization $m(t)$. The value of magnetization remains small under local control, whereas it becomes significantly larger under both optimal control methods (simulated annealing and quantum annealing). For each method, at $\alpha = 0.8$, the response of the magnetization oscillates or fluctuates around zero. To confirm this observation, the time average of the magnetization of Eq. (18), denoted as \bar{m} , is plotted in Fig. 5(b). Here, the ferromagnetic transition at $\alpha \rightarrow 1$, that is, the finite value of \bar{m} , is observed for the magnetization under local control, which was originally reported in Ref. [26]. Also, under optimal control, the time average of the magnetization \bar{m} takes a large value when $\alpha \rightarrow 1$, which shows that a ferromagnetic transition similar to that under local control occurs under optimal control.

In addition to the ferromagnetic transition, the large amplitudes observed under optimal control are indeed a quantification of the synchronization of proximity signals observed in Fig. 2. For further analysis of this synchronization, we also evaluate two types of autocorrelation functions. Figure 6(a) shows the autocorrelation function obtained from the time-series data of the signal state $\sigma_i(t)$ for $t \in [0, 200]$. Here, the autocorrelation function is computed at all intersections, and the average value is displayed in Fig. 6(a). Under local control, there is a negative correlation peak around $t = 3$, which means that the signals switch approximately every 3 time steps. In contrast, under optimal control, the negative correlation peak is in the interval of $t = [10, 15]$ steps, and the same state is maintained for a time longer than that under local control. Next, Fig. 6(b) shows the correlation between the display of signals at one intersection and another intersection, with the distance between the intersections as a parameter. Here, the correlation function is calculated for all the intersections for fixed time $t = 100$, and the average value thereof is plotted. In Fig. 6(b), the distance is normalized to make the distance of adjacent intersections equal to 1. There is almost no correlation between adjacent signals under local control, while there is a positive correlation of up to 4–6 adjacent intersections under optimal control.

Then, we extract quantities from these correlation functions to investigate the effect of α . First, considering that both the temporal and spatial autocorrelations in Fig. 6 decay while oscillating, both functions are fitted with the following equation:

$$R(z) = \exp(-\lambda z) \cos(\omega z), \quad (19)$$

where λ represents the damping rate coefficient, ω represents the vibration frequency coefficient, and $z \in \mathbb{R}_+$ represents different variables, i.e., the time t for the time autocorrelation function and the distance between intersections for the spatial autocorrelation function. Figure 7(a) plots ω values obtained by fitting Eq. (19) to the time autocorrelation, as a function of α . Under local control, the vibration frequency is $\omega \approx 1$ regardless of the value of α , while ω decreases as α increases under optimal control. That is, the period of oscillation increases as the vehicle straight driving rate increases. Next, we show in Fig. 7(b) the value of λ obtained by fitting Eq. (19) to the spatial autocorrelation, as a

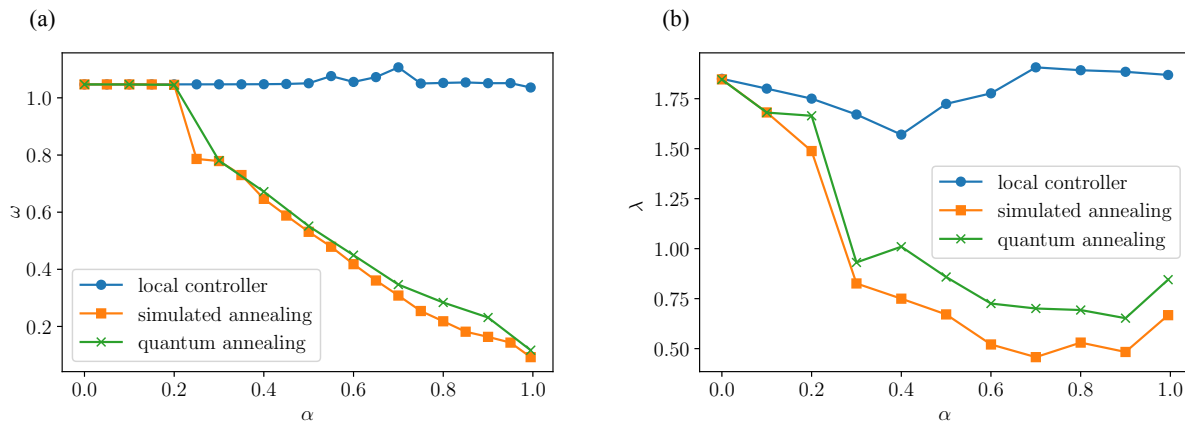


FIG. 7. Parameters extracted from time and spatial autocorrelations, as functions of α for different control methods. (a) Time autocorrelation function frequency ω versus α and (b) Radially averaged autocorrelation decay rate λ versus α . Parameters η and L are fixed as $\eta = 1.0$ and $L = 50$, respectively.

function of α . Under local control, the correlation decreases with an attenuation factor of $\lambda \approx 1.75$, regardless of the value of α . In contrast, under optimal control, λ decreases as α increases, which means that the signal displays between the more distant intersections remain correlated. These observations show that the synchronization of proximity signals in time and space becomes important for achieving a balanced traffic flow as the probability of vehicles going straight increases.

METHODS

Parameter Identification for Objective Function

As stated in *Discussion*, a direct correspondence between the optimal control and local control is established for small values of α , with the apparent relation $\theta = \eta$ between the local control switching constant θ in Eq. (11) and the optimal control weight parameter η in Eq. (4). To make a systematic comparison for an arbitrary value of α , however, we still need to construct a protocol to determine the values of θ and η . The strategy is described as follows. Given a value of η , we select a value of θ , denoted by $\hat{\theta}$, from a candidate set Θ via the following auxiliary numerical analysis:

1. For one value of θ in the set Θ , numerical simulation using local control (11) is performed to obtain time series data $\mathbf{x}(t)$ and $\boldsymbol{\sigma}(t)$. The value of the objective function (4) using the given η is calculated from the obtained time series data. This time average value is denoted as $\bar{H}(\theta)$.
2. Step 1 is performed for all θ in Θ to find the $\hat{\theta}$ that minimizes the time average value \bar{H} , that is, $\hat{\theta} = \arg \min_{\theta \in \Theta} \bar{H}(\theta)$.

We plot the result of the above procedure in Fig. 8. Figure 8(a) shows \bar{H} against θ when η is fixed as $\eta = 1.0$. When $\alpha = 0$, \bar{H} is a convex function and indeed $\hat{\theta} \approx \eta$ is satisfied. However, for larger values of α , \bar{H} becomes non-convex, and particularly for $\alpha = 0.995$, the relation $\hat{\theta} = \eta$ no longer holds. Figure 8(b) shows the value of $\hat{\theta}$ that minimizes \bar{H} versus η for the interval $\eta \in [0.0, 3.0]$. When $\alpha = 0$, the linear relation $\hat{\theta} = \eta$ approximately holds, but when $\alpha \neq 0$, this relation breaks down and some discontinuities appear. These discontinuities correspond to the changes in the local minima observed in Fig. 8(a).

Decomposition of Objective Function

The D-Wave 2000Q is capable of using up to 2,048 qubits. Each qubit is *not* coupled with all the other qubits; instead, the assemblage has a *chimera structure*, in which closely connected 8-bit units are arranged vertically and horizontally [29]. For this reason, the variables of a given Hamiltonian cannot be directly assigned to physical qubits in the annealing machine. The method of converting the given graph structure to the chimera structure is called *minor*

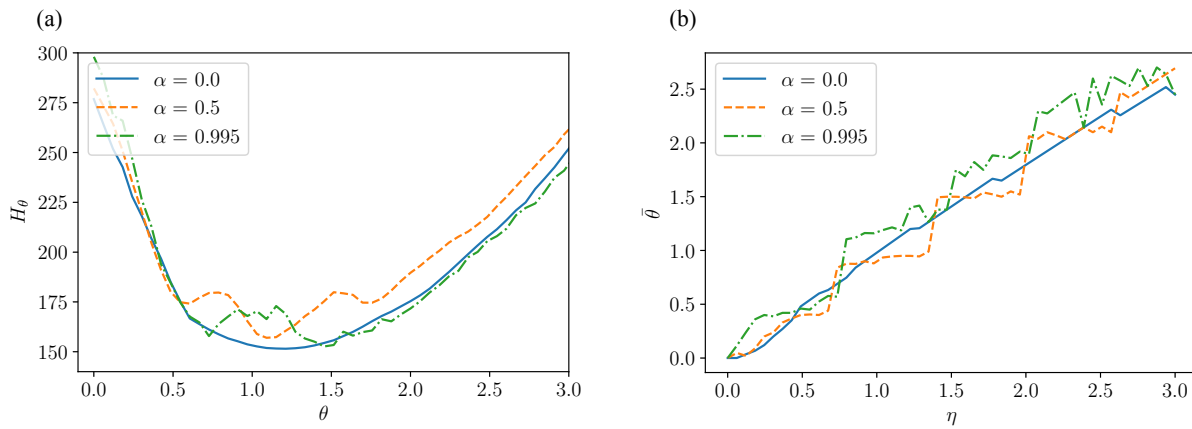


FIG. 8. Correspondence between η and θ . (a) Time average of the objective function \bar{H} versus θ , when the value of η is fixed as $\eta = 1.0$. The cases with $\alpha \in \{0.0, 0.5, 0.995\}$ are shown. (b) $\hat{\theta}$ versus η for $\alpha \in \{0.0, 0.5, 0.995\}$.

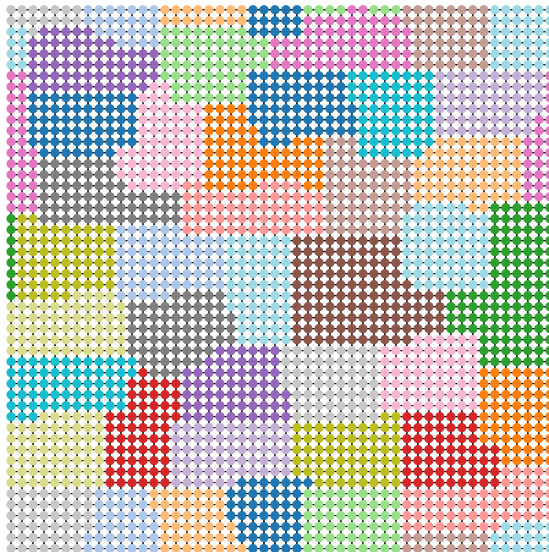


FIG. 9. Graph partitioning using Metis. Each node represents a component of the Hamiltonian coefficient matrix J in Eq. (10), and the color of each node indicates the group to which the component belongs.

embedding; this structure is realized by expressing one logical variable with strongly coupled multiple physical qubits. In the chimera structure, $N^2/4$ physical qubits are necessary for solving a fully connected N -variable problem, which means that the maximum number of variables that the 2000Q is capable of handling is as small as 64 when the original problem has a fully connected structure. This implies that $L^2 \leq 64 \Leftrightarrow L \leq 8$ must be satisfied for the number of roads L .

A method exists for solving a problem that exceeds the above limitation: to divide the Hamiltonian variable of Eq. (10) into several groups and minimize the approximate Hamiltonian for each group. We define the traffic signal state vector of the j th group as $\boldsymbol{\sigma}^j := [\sigma_{i_1}, \sigma_{i_2}, \dots, \sigma_{i_m}]^\top$, where i_1, i_2, \dots, i_m are subscripts of variables included in the j th group. Then, we define the Hamiltonian of the group j as

$$H^j(\boldsymbol{\sigma}^j(t)) := \boldsymbol{\sigma}^j(t)^\top J_{jj} \boldsymbol{\sigma}^j(t) + (h_j + \boldsymbol{\sigma}^{\bar{j}}(t)^\top J_{\bar{j}j}) \boldsymbol{\sigma}^j(t), \quad (20)$$

where J_{jj} is a matrix extracting the (j, j) th components of matrix J in Eq. (10). Similarly, h_j is a vector obtained by extracting the j th component of h . The index \bar{j} represents the set of variables *not* belonging to group j . One naive approximation is to regard the variables outside group j as constant. This allows the annealing machine to deal with a Hamiltonian exceeding the limitation, but at the same time this approach degrades the control performance. To reduce

such errors, the variables having a large interaction should be in the same group, and the variable interaction between different groups should be small. Such a problem is called a *graph partitioning problem*, which is known to be an NP-hard problem, but there are some approximation methods with adequate accuracy. For the actual implementation, we used the *Metis* software, which is a widely used solver for graph partitioning problems, to break up the large-scale problem into several groups having fewer than 64 variables [30]. Figure 9 shows the result of the graph partitioning of the city of $L = 50$ into 42 groups using Metis, where we certainly see that the adjacent intersections, i.e., the strongly interacting variables, are included in the same group.

-
- [1] Zhang, J. *et al.* Data-Driven Intelligent Transportation Systems: A Survey. *IEEE Transactions on Intelligent Transportation Systems* **12**, 1624–1639, DOI: 10.1109/TITS.2011.2158001 (2011).
- [2] Bishop, R. *Intelligent Vehicle Technology and Trends* (Artech House, 2005).
- [3] Cheng, X., Yang, L. & Shen, X. D2D for Intelligent Transportation Systems: A Feasibility Study. *IEEE Transactions on Intelligent Transportation Systems* **16**, 1784–1793, DOI: 10.1109/TITS.2014.2377074 (2015).
- [4] Papageorgiou, M., Diakaki, C., Dinopoulou, V., Kotsialos, A. & Yibing Wang. Review of Road Traffic Control Strategies. *Proceedings of the IEEE* **91**, 2043–2067, DOI: 10.1109/JPROC.2003.819610 (2003).
- [5] Wei, H., Zheng, G., Gayah, V. & Li, Z. A Survey on Traffic Signal Control Methods. *arXiv:1904.08117 [cs, stat]* (2019). 1904.08117.
- [6] Koonce, P. & Rodegerdts, L. Traffic Signal Timing Manual. Tech. Rep., United States. Federal Highway Administration (2008).
- [7] Roess, R. P., Prassas, E. S. & McShane, W. R. *Traffic Engineering* (Pearson/Prentice Hall, 2004).
- [8] Varaiya, P. The Max-pressure Controller for Arbitrary Networks of Signalized Intersections. In Ukkusuri, S. V. & Ozbay, K. (eds.) *Advances in Dynamic Network Modeling in Complex Transportation Systems*, 27–66, DOI: 10.1007/978-1-4614-6243-9_0082 (Springer New York, New York, NY, 2013).
- [9] Hunt, P. B., Robertson, D. I., Bretherton, R. D. & Winton, R. I. Scoot - A Traffic Responsive Method of Coordinating Signals. *Publication of: Transport and Road Research Laboratory* (1981/00/00).
- [10] Arel, I., Liu, C., Urbanik, T. & Kohls, A. G. Reinforcement Learning-based Multi-agent System for Network Traffic Signal Control. *IET Intelligent Transport Systems* **4**, 128–135, DOI: 10.1049/iet-its.2009.0070 (2010).
- [11] Nishi, T., Otaki, K., Hayakawa, K. & Yoshimura, T. Traffic Signal Control Based on Reinforcement Learning with Graph Convolutional Neural Nets. In *2018 21st International Conference on Intelligent Transportation Systems (ITSC)*, 877–883, DOI: 10.1109/ITSC.2018.8569301 (IEEE, 2018).
- [12] Khamis, M. A., Gomaa, W. & El-Shishiny, H. Multi-objective Traffic Light Control System Based on Bayesian Probability Interpretation. In *2012 15th International IEEE Conference on Intelligent Transportation Systems*, 995–1000, DOI: 10.1109/ITSC.2012.6338853 (IEEE, 2012).
- [13] Faouzi, N.-E. E., Leung, H. & Kurian, A. Data Fusion in Intelligent Transportation Systems: Progress and Challenges – A Survey. *Information Fusion* **12**, 4–10, DOI: 10.1016/j.inffus.2010.06.001 (2011).
- [14] Kadowaki, T. & Nishimori, H. Quantum Annealing in the Transverse Ising Model. *Physical Review E* **58**, 5355–5363, DOI: 10.1103/PhysRevE.58.5355 (1998).
- [15] Johnson, M. W. *et al.* Quantum Annealing with Manufactured Spins. *Nature* **473**, 194–198, DOI: 10.1038/nature10012 (2011).
- [16] Inoue, D. & Yoshida, H. Model Predictive Control for Finite Input Systems using the D-Wave Quantum Annealer. *Scientific Reports* **10**, 1–10, DOI: 10.1038/s41598-020-58081-9 (2020).
- [17] King, J., Yarkoni, S., Nevisi, M. M., Hilton, J. P. & McGeoch, C. C. Benchmarking a Quantum Annealing Processor with the Time-to-Target Metric. *arXiv:1508.05087 [quant-ph]* (2015). 1508.05087.
- [18] McGeoch, C. C. & Wang, C. Experimental Evaluation of an Adiabatic Quantum System for Combinatorial Optimization. In *Proceedings of the ACM International Conference on Computing Frontiers, CF '13*, 23, DOI: 10.1145/2482767.2482797. ACM (Association for Computing Machinery, Ischia, Italy, 2013).
- [19] Venturelli, D., Marchand, D. J. J. & Rojo, G. Quantum Annealing Implementation of Job-Shop Scheduling. *arXiv:1506.08479 [quant-ph]* (2016). 1506.08479.
- [20] O’Malley, D., Vesselinov, V. V., Alexandrov, B. S. & Alexandrov, L. B. Nonnegative/Binary Matrix Factorization with a D-Wave Quantum Annealer. *PLOS ONE* **13**, e0206653, DOI: 10.1371/journal.pone.0206653 (2018).
- [21] Ohzeki, M., Okada, S., Terabe, M. & Taguchi, S. Optimization of Neural Networks Via Finite-Value Quantum Fluctuations. *Scientific Reports* **8**, 1–10, DOI: 10.1038/s41598-018-28212-4 (2018).
- [22] Yang, C. N. The Spontaneous Magnetization of a Two-Dimensional Ising Model. *Physical Review* **85**, 808–816, DOI: 10.1103/PhysRev.85.808 (1952).
- [23] McCoy, B. M. & Wu, T. T. *The Two-Dimensional Ising Model* (Courier Corporation, 2014).
- [24] Binder, K. Finite Size Scaling Analysis of Ising Model Block Distribution Functions. *Zeitschrift für Physik B Condensed Matter* **43**, 119–140, DOI: 10.1007/BF01293604 (1981).
- [25] Glauber, R. J. Time-Dependent Statistics of the Ising Model. *Journal of Mathematical Physics* **4**, 294–307, DOI: 10.1063/1.1703954 (1963).
- [26] Suzuki, H., Imura, J.-i. & Aihara, K. Chaotic Ising-Like Dynamics in Traffic Signals. *Scientific Reports* **3**, 1–6, DOI:

10.1038/srep01127 (2013).

- [27] Suman, B. & Kumar, P. A Survey of Simulated Annealing as a Tool for Single and Multiobjective Optimization. *Journal of the Operational Research Society* **57**, 1143–1160, DOI: 10.1057/palgrave.jors.2602068 (2006).
- [28] Hamerly, R. *et al.* Experimental Investigation of Performance Differences Between Coherent Ising Machines and a Quantum Annealer. *Science Advances* **5**, DOI: 10.1126/sciadv.aau0823 (2019).
- [29] Boothby, T., King, A. D. & Roy, A. Fast Clique Minor Generation in Chimera Qubit Connectivity Graphs. *Quantum Information Processing* **15**, 495–508, DOI: 10.1007/s11128-015-1150-6 (2016).
- [30] Karypis, G. & Kumar, V. A Fast and High Quality Multilevel Scheme for Partitioning Irregular Graphs. *SIAM Journal on Scientific Computing* **20**, 359–392 (1998).

ACKNOWLEDGEMENTS

The authors would like to thank Dr. Kiyosumi Kidono of Toyota Central R&D Labs. for the useful discussions.